Title

ANGULAR-MOMENTUM EFFECTS ON NEUTRON EMISSION BY Dy156, Tb153, AND Tb157 COMPOUND NUCLEI

Authors

Simonoff, Gabriel N.
Alexander, John M.

Publication Date

1962-02-26

UCRL-10099

University of California

Ernest O. Lawrence Radiation Laboratory

Berkeley, California

DISCLAIMER

UCRL-10099

UNIVERSITY OF CALIFORNIA
Lawrence Radiation Laboratory
Berkeley, California

Contract No. W-7405-eng-48

ANGULAR-MOMENTUM EFFECTS ON NEUTRON EMISSION BY Dy^{156}, Tb^{153}, AND Tb^{157} COMPOUND NUCLEI

Gabriel N. Simonoff and John M. Alexander

February 26, 1962

ANGULAR-MOMENTUM EFFECTS ON NEUTRON EMISSION BY Dy^{156}, Tb^{153}, and Tb^{157} COMPOUND NUCLEI *

Gabriel N. Simonoff[† ‡] and John M. Alexander

Lawrence Radiation Laboratory
University of California
Berkeley, California

February 26, 1962

I. INTRODUCTION

It is very difficult to directly observe the effect of angular momentum on the decay of an excited nucleus. First, there must be a verification of the excitation energy and angular momentum of the excited nucleus. Second, one would like to be able to vary these quantities separately, and observe the decay properties. To date it has not been possible to attain this goal. In this work we make measurements of the cross section and recoil properties of the following: (a) Dy nuclides produced by neutron evaporation from Dy^{156} compound nuclei; (b) Tb^{149g} produced by neutron evaporation from Tb^{153} and Tb^{157} compound nuclei. It has recently been established that Tb^{149} has a 4.0-min isomeric state that has a very small probability of decaying to the ground state.[1] It is reasonable to suppose that neutron emission from the compound nuclei of higher angular momentum leads to 4.0-min Tb^{149m} and that only those compound nuclei of lower angular momentum decay to Tb^{149g}.[2] Comparison of the properties of these two classes of reactions reveals certain striking differences that we attribute to the effect of angular momentum.

Many studies of nuclear reactions have been interpreted in terms of a two-stage mechanism. The first stage is a fast initial interaction described by a nucleon-nucleon collision cascade[3] or, for lower incident energies, by compound-

nucleus formation.[4] The second stage is the decay of the excited nuclei so formed, and is described by the statistical model.[5] However, the basic assumptions of compound-nucleus or nucleon-cascade models have been subjected to very few experimental tests. The observation of particles emitted with angular distributions symmetric about $\pi/2$ in the center-of-mass (c.m.) system is usually taken as sufficient evidence for compound-nucleus formation. (It has been pointed out that this symmetry is not a necessary condition for decay of a compound nucleus, but in most cases it is sufficient.[6]) The fact is that most experimental observations of the angular distributions of protons, helium ions, etc. indicate that some particles are emitted with symmetric angular distributions, but usually asymmetric components are observed.[7] Thus it has been difficult to study the properties of highly excited compound nuclei, because of possible interference by noncompound-nucleus processes.

Recently, radiochemical recoil range techniques have proved to be a valuable tool for testing the formation of a compound nucleus.[8,9,10] Evidence has been presented that a large class of heavy-ion-induced reactions proceed by a pure compound-nucleus mechanism.[10]

In this study we have measured a variety of features for several nuclear reactions: (a) average range values, which test compound-nucleus formation; (b) angular and range distributions, which reflect the angular and energy distributions of the emitted neutrons, and (c) excitation functions, which reflect the energy dependence of the probability for various decay chains. The nuclides Tb^{149g}, Dy^{150}, and Dy^{151} have been observed from C^{12} reacting with Nd^{144}, and from O^{16} reacting with Ce^{140} — both reactions leading to Dy^{156} compound systems. The product 4.1-hr Tb^{149g} has been studied from C^{12} reacting with Pr^{141} to form the compound system Tb^{153}, and from B^{11} reacting with Nd^{146} to form Tb^{157}.

The nuclide 4.1-hr Tb^{149g} has a 4-min isomeric state of higher spin. This 4-min Tb^{149m} has a very low [illegible] branching ratio for isomeric transition

to the ground state.[1] The decay properties of Dy^{149} are not known, but it is believed that this nuclide decays by positron emission and electron capture to 4.1-hr Tb^{149g} and 4-min Tb^{149m} in the ratio of approximately 1:2.[11]

The cross section data for (HI,xn)Tb^{149g} indicate that direct formation of Tb^{149g} is improbable. Therefore it is likely that the 4.1-hr $_{65}Tb^{149g}$ formed from $_{66}Dy$ compound nuclei comes almost entirely from the decay of Dy^{149}. In this report we assume that this is the case and refer to the properties of the 4.1-hr Tb^{149g} observed from Dy^{156} compound nuclei as Dy^{149}. We can infer from these properties of the radioactive decay that Tb^{149g} formed from Tb compound nuclei reflects the properties of only those compound nuclei of low angular momentum. The excited nuclei of high angular momentum will probably decay by particle and photon emission to the higher spin states of the final products.[2] Thus the 4-min Tb^{149m} probably shields 4.1-hr Tb^{149} from formation by decay of high-spin-compound nuclei.

The compound nuclei that we study may be classified in two groups: (a) low-spin Tb compound nuclei that produce 4.1-hr Tb^{149g}, and (b) Dy compound nuclei, of normal spin distribution, that produce Dy^{149}, Dy^{150}, and Dy^{151}.

II. RECOIL EFFECTS OF THE COMPOUND-NUCLEUS MECHANISM

The basic features of the compound-nucleus mechanism are the following. A projectile and a target nucleus interact to form an excited compound system having a mean life that is long compared to the time required for the projectile to traverse the nuclear diameter.[4] The excited compound nucleus decays by emitting particles and photons until a stable or radioactive final product is formed.[5] The angular distribution of the emitted particles or photons will be symmetric about $\pi/2$ in the frame of the compound nucleus if the level density of the residual nucleus is large enough to justify the random-phase approximation.[6]

In this work we study systems with initial excitation energies ≈50 to 125 Mev, and thus we assume that this approximation is justified. If the angular momenta of the emitted waves are very large, then the angular distribution approaches $1/\sin\theta$; if only $\ell=0$ waves are emitted, then isotropy results.[6]

Let us consider in detail the consequences of this mechanism for the following recoil properties of the final products: (a) average range R_o, (b) range straggling parameter ρ, and (c) root-mean-square angle (lab system), $\langle\theta_L^2\rangle^{1/2}$. Let $\underset{\sim}{v}$ denote the velocity given the compound nucleus by the initial impact of the projectile (this is identical to the velocity of the center of mass). Let $\underset{\sim}{V}$ denote the velocity in the c.m. system given to the final product by the evaporation of particles. Let θ denote the c.m. angle between $\underset{\sim}{v}$ and $\underset{\sim}{V}$ and θ_L denote the lab angle between $\underset{\sim}{v}$ and $\underset{\sim}{v} + \underset{\sim}{V}$. The angular distribution of $\underset{\sim}{V}$ is designated by $W(\theta)$, and the recoil distance is taken as equal to $k|\underset{\sim}{v} + \underset{\sim}{V}|^N$, where k and N are constants.

As has been previously discussed,[8] the measured average range (the average projection of the recoil distances on the beam direction) is described as follows:

$$R_o = \frac{k}{2} \int_0^{\pi} (v^2 + V^2 + 2vV\cos\theta)^{N/2} \cos\theta_L \, W(\theta) \sin\theta \, d\theta. \qquad (1)$$

For $V \ll v$, and $W(\theta) = 1$ we have

$$R_o = kv^N \left[1 + \frac{1}{6}(N^2 + N - 2)(V/v)^2 + \ldots\right], \qquad (2)$$

and for $W(\theta) \propto 1/\sin\theta$ we have

$$R_o = kv^N \left[1 + \frac{1}{4}(N^2-1)(V/v)^2 + \ldots\right]. \qquad (3)$$

If the average quantity $\langle V^2\rangle \ll v^2$ and $W(\theta)$ is symmetric about $\pi/2$, then R_o can be considered to depend only on v, k, and N — and to be independent of V and $W(\theta)$. Then the average recoil range of the product should be associated with a recoil energy E_R such that

$$E_R = \frac{E_b A_b A_R}{(A_b + A_T)^2} , \tag{4}$$

where mass number is denoted by A with subscripts as follows: b, the bombarding particle; R, the recoil atom or final product; and T, the target. The kinetic energy of the projectile in the laboratory system is denoted by E_b.

The contribution to the measured range straggling from the distribution of $\underset{\sim}{v} + \underset{\sim}{V}$ is given by

$$\langle (R-R_0)^2 \rangle = \frac{1}{2} \int_0^{\pi} [R(v,V,\theta) - R_0]^2 \, W(\theta) \sin\theta \, d\theta \tag{5}$$

For $V \ll v$, and for $W(\theta) = 1$ we have [to order $(V/v)^3$]

$$\frac{\langle (R-R_0)^2 \rangle}{R_0^2} = \frac{N^2 \langle V^2 \rangle}{3v^2} \tag{6}$$

and for $W(\theta) = a + b\cos^2\theta$,

$$\frac{\langle (R-R_0)^2 \rangle}{R_0^2} = \frac{N^2 \langle V^2 \rangle [1+(3b/5a)]}{3v^2 [1+(b/3a)]} , \tag{7}$$

and for $W(\theta)$ proportional to $1/\sin\theta$ we have

$$\frac{\langle (R-R_0)^2 \rangle}{R_0^2} = \frac{N^2 \langle V^2 \rangle}{2v^2} . \tag{8}$$

Detailed calculations by the Monte Carlo method have shown that for $V^2 \ll v^2$ the range distribution due to evaporation effects can be closely approximated by a Gaussian distribution with straggling parameter denoted by ρ_n.[12] Thus we have

$$\rho_n^2 = \frac{\langle (R-R_0)^2 \rangle}{R_0^2} \tag{9}$$

The average square of the angle $\langle\theta_L^2\rangle$ of the recoil atoms is given by

$$\langle\theta_L^2\rangle = \frac{1}{2}\int_0^{\pi}\left\{\tan^{-1}\left(\frac{V\sin\theta}{v+V\cos\theta}\right)\right\}^2 W(\theta)\sin\theta\, d\theta. \qquad (10)$$

To order $(V/v)^3$ for $W(\theta) = 1$ we have

$$\langle\theta_L^2\rangle = \frac{2\langle V^2\rangle}{3v^2}. \qquad (11)$$

For $W(\theta) = a + b\cos^2\theta$ we have

$$\langle\theta_L^2\rangle = \frac{2\langle V^2\rangle[1+(b/5a)]}{3v^2[1+(b/3a)]}. \qquad (12)$$

For $W(\theta)$ proportional to $1/\sin\theta$ we have

$$\theta_L^2 = \frac{\langle V^2\rangle}{2v^2} \qquad (13)$$

The equations given above show relationships between some observable properties and the magnitudes of the velocities v and V. The velocity v is, of course, specified by the momentum of the projectile and the mass of the compound nucleus

$$v^2 = \frac{2A_b E_b}{(A_b+A_T)^2}. \qquad (14)$$

The value of $\langle V^2\rangle$ is determined by the average total kinetic energy T_n of the emitted particles in the c.m. system, and by their angular distribution. The recoil velocity due to emission of photons can be neglected.

If the compound nucleus emits nucleons in random directions then $W(\theta) = 1$, and we have

$$\langle V^2\rangle = \frac{8T_n}{(A_T+A_b+A_R)^2}. \qquad (15)$$

The total energy available in the c.m. system is $E_b A_T/(A_b+A_T) + Q$ and therefore the average total energy emitted as photons T_γ is

$$T_\gamma = \left[\frac{E_b A_T}{(A_b+A_T)}\right] + Q - T_n. \qquad (16)$$

Thus from Eqs. (6), (9), and (15) we have

$$\rho_n^2 = \frac{4N^2 T_n (A_b + A_T)^2}{3E_b A_b (A_b + A_T + A_R)^2}, \qquad (17)$$

and from Eqs. (11) and (15) we have

$$\langle\theta_L^2\rangle = \frac{(8T_n)(A_b + A_T)^2}{(3E_b A_b)(A_b+A_T+A_R)^2}. \qquad (18)$$

If the angular distribution of the emitted particles is not isotropic the mathematics is much more complicated. However, from Eqs. (8) and (13) one can see that even an extreme case of $W(\theta) \propto 1/\sin\theta$ leads to changes of only about 25% in ρ_n, and about 15% in $\langle\theta_L^2\rangle^{1/2}$.

III. EXPERIMENTAL TECHNIQUES AND RESULTS

In our experiments we have made observations of the nuclides 4.1-hr Tb^{149g}, 7.4-min Dy^{150}, and 17.9-min Dy^{151}. These are the only alpha-emitting nuclides in the rare-earth region that have convenient decay periods and favorable alpha branching ratios. Therefore, measurement of the alpha radioactivity by ionization chambers allows us to identify these specific products without chemical analysis.

A. Range Measurements

The range measurements were made with thin targets (30 to 100μg/cm^2), and thin Al catcher foils ≈ 150μg/cm^2), as described previously.[8] On a probability scale F_t, the fraction of the total activity that passed through catcher foils of combined thickness t was plotted against t. These probability plots always indicate that the range distribution can be described as a Gaussian function with two parameters (the average range R_0 and the straggling parameter ρ):

$$P(R)dR = \frac{1}{R_0 \rho (2\pi)^{1/2}} \exp\left[-\left(\frac{R-R_0}{\sqrt{2}\,R_0\,\rho}\right)^2\right] dR$$

The results of the range measurements are given in Table I. The first three columns give the reaction, beam energy, and observed product, respectively. The values of the measured quantities R_0 and ρ are given in the fourth and fifth columns. The measured straggling parameter is the result of contributions from several sources: (a) finite target thickness ρ_W, (b) catcher-foil inhomogeneities ρ_f, (c) inherent straggling in the stopping process ρ_s, and (d) the nuclear reaction ρ_n. If all these contributions are treated as Gaussian we have

$$\rho_n^2 = \rho^2 - \rho_W^2 - \rho_f^2 - \rho_s^2 .$$

The effects of ρ_W, ρ_f, and ρ_s have been subtracted as previously described,[10] and we show the values of ρ_n in the last column.

The values of ρ_n are not accurate enough to use in a quantitative way. We can only say that the values of ρ_n are not inconsistent with any conclusions deduced from the angular-distribution results. As shown in Eqs. (17) and (18) the values of ρ_n and $\langle\theta_L^2\rangle^{1/2}$ are both related to T_n.

B. Cross-Section Measurements

An accurate cross-section measurement requires measurement of the target thickness, beam intensity, and disintegration rate of the desired nuclide. Targets were prepared by evaporation of rare-earth metals ($\approx$ 36 to 100$\mu g/cm^2$) onto 0.00025-in. Al foils. The Al foils were weighed before and after evaporation and the relative thicknesses of the target layers were determined to $\pm$ 1 $\mu g/cm^2$. We assumed that the chemical forms of the layers at the time of weighing were CeO_2 and Nd_2O_3. We plan to check this assumption by chemical analysis. The Nd^{144} and Nd^{146} and Ce^{140} targets were prepared from enriched isotopes obtained from The Oak Ridge National Laboratory. The enrichments were 97.3% Nd^{144}, 96.2% Nd^{146} and 99.6% Ce^{140}.

All cross sections were measured by the stacked-foil technique. The range measurements demonstrate that all the product atoms recoil from the target layers into the catcher foils. Counting was performed on 10 to 14 ionization chambers of 2π geometry. The efficiencies of the ionization chambers were intercalibrated with thick uranium standards. For measurements in which thin Al foils ($\approx$ 0.15 mg/cm^2) were used, no absorption correction was applied, and the counting efficiency was taken as 50%. For most cross-section measurements, thick Al catcher foils ($\approx$ 1.8 mg/cm^2) were used. In these cases an absorption correction of $[1 - (d/r)]^{-1}$ was applied, where d denotes the average depth of the product atoms, and r denotes the effective range of the alpha particles from the various nuclides. The values of d were taken from interpolations of the measured average recoil ranges. The value of r for Tb^{149} was measured as described elsewhere.[11] The decay periods and alpha branching ratios were taken as follows: 4.1-hr Tb^{149g}, 10% α;[13] 7.4-min Dy^{150}, 17.9% α; 17.9 min Dy^{151}, 6.2% α.[14]

The cross-section data are given in Table II. Bombarding energies were calculated from the range-energy curves of Northcliff[15] and the maximum Heavy-Ion Linear Accelerator (Hilac) energy of 10.38 Mev/nucleon.[16]

C. Angular-Distribution Measurements

The angular-distribution measurements were performed by essentially the same method developed by Harvey et al.[9] A thin target layer was exposed to a collimated beam from the Berkeley Hilac. A thick (0.001-in.) Al catcher foil was placed at some distance from the target, and circular rings were cut from the catcher concentric about the beam. The geometry of the apparatus is shown in Fig. 1. The angular resolution of the beam was defined by two 1/16-in. collimators to less than 0.5 deg in most experiments. In a few experiments the second collimator was 1/8 in. in diameter, giving rise to an angular definition

of $\approx$ 1 deg. The effect of the size of the second collimator was measured experimentally (see Table IV). The catcher foil was cut by a stainless steel cutter and a hydraulic press into rings of 1/8-in. radial dimension. Each ring subtended $\approx$ 1 deg. A careful calibration of the dimensions of the two cutters was performed by weighing several sets of rings cut from sheets of uniform Al foil. The angles defined by each ring are given in Table III.

For comparison with the measurements of Morton,[17] two experiments were done for the reaction $Pr^{141}(C^{12},4n)Tb^{149}$. A direct comparison is shown in Fig. 2. Our experiments indicate a stronger change in the angular distribution between the incident energies of 58 and 68 Mev. We attribute this difference to the much poorer angular resolution of his experiment. In addition, Morton did not define the beam angle with two collimators, nor correct for scattering in the target layer. These combined effects lead to significant corrections to the average or root mean square angle as will be shown later. Considering these experimental differences the comparison is adequate.

The results of all angular-distribution measurements are given in Table IV. The first two columns give the beam energy and target thickness, respectively. As shown in Table III, the two cutters had slightly different dimensions. Therefore, for each experiment we give the cutter and, for each ring, the fractional cross section per unit angle $\Delta\sigma/\sigma\Delta\theta$. The average angle $\langle\theta_L\rangle$ was calculated by the relationship

$$\langle\theta_L\rangle = \sum_i (\Delta\sigma_i/\sigma)\bar{\theta}_i ,$$

where $\bar{\theta}_i$ is the mean angle of each ring and $\Delta\sigma_i/\sigma$ is the fraction of the total activity observed in each ring. The root mean square angle was similarly calculated:

$$\langle\theta_L^2\rangle^{1/2} = \left[\sum_i (\Delta\sigma_i/\sigma)\, \overline{\theta_i^2} \right]^{1/2} ,$$

where $\overline{\theta_i^2}$ is the mean squared angle of each ring. Values of $\Delta\sigma_i$ less than 2% of the maximum value of $\Delta\sigma_i$ were not included in the summations.

The effect of target thickness on the angular distribution of Tb^{149} was carefully studied for several cases. One series of these experiments is shown in Fig. 3. The values of $\langle\theta_L\rangle$ and $\langle\theta_L^2\rangle^{1/2}$ change significantly but not very rapidly with target thickness, as shown in Fig. 4. We have used the values of $d\langle\theta\rangle/dW$ and $d\langle\theta^2\rangle^{1/2}/dW$ shown in Fig. 4 to correct these average properties to zero target thickness. The assumption was made that all reactions of the same projectile have the same value of $d\langle\theta\rangle/dW$ and $d\langle\theta^2\rangle^{1/2}/dW$. This is probably a very good approximation (especially for the C^{12} and O^{16} experiments) because the angular distributions and recoil velocities are very similar. The detailed angular distributions in Table IV for W=0 were obtained by linearly extrapolating $\Delta\sigma/\sigma\Delta\theta$ to W=0 for each ring. This procedure becomes more uncertain, of course, with increasing angle.

IV. DISCUSSION

A. Ranges

In preceding papers we have presented an internal-consistency argument for using average range values to test the validity of the compound-nucleus model.[8,10] The lack of independent range-energy data for heavy recoil atoms necessitates this kind of treatment. First, assume that the compound-nucleus mechanism is valid. Thus Eq. (4) should give the recoil energy E_R appropriate to the average range R_0. Then the values of R_0 are plotted versus E_R, as in Fig. 5. From this figure we see that one smooth curve fits all the measurements. Furthermore, this curve is the same that is consistent with Tb^{149} range measurements from many other reactions. This test implies that Eq. (4) gives a correct description of the recoil energy or, in other words, that the projectile transfers all its momentum to the compound system. We conclude that the most likely

mechanism for all these reactions is compound-nucleus formation, followed by emission of particles with forward-backward symmetry. All further discussion is based on this conclusion.

B. Excitation Functions

We have measured excitation functions for the production of Tb^{149}, Dy^{150}, and Dy^{151} in several reactions. These measurements depend on the total cross section for compound-nucleus formation σ_{CN}, and the probability that an excited compound nucleus will decay to the observed product. There is evidence that the total reaction cross section σ_R, for heavy-ion reactions can be calculated adequately by simple barrier penetration of a parabolic well.[18] It is clear that some reactions do not proceed by compound-nucleus formation. But the abundance of these noncompound-nucleus reactions is not known. For the purpose of this discussion we will use calculations of the total reaction cross section as if they represented the cross section for compound-nucleus formation. The arguments will be significantly altered only if there is a strong energy dependence of σ_{CN}/σ_R.

The two reactions $Ce^{140} + O^{16}$ and $Nd^{144} + C^{12}$ both produce the compound nucleus Dy^{156}. The decay of this compound nucleus is expected to be dependent on its excitation energy and its total angular momentum J. We can investigate the J dependence of the decay by comparing the fractional reaction cross sections for Tb^{149}, Dy^{150}, and Dy^{151} at various excitation energies. Such a comparison is shown in Fig. 6. We see that the fractional excitation functions are very similar, with a very small shift to somewhat higher energies for the O^{16}-induced reactions.

We conclude that the decay probabilities of the compound nucleus Dy^{156} are not very sensitive to the differences in angular momentum deposited by C^{12} and O^{16} projectiles.

Another very interesting feature of these reactions can be obtained by plotting the fractional reaction cross section as a function of the total energy per nucleon available for decay. These plots are shown in Fig. 7 and 8. The excitation functions for Dy compound nuclei all peak at about 5 to 6 Mev per emitted neutron. This is quite a different result from that observed for Tb^{149g} produced from Tb compound nuclei. These reactions have been shown to peak at 3 to 4 Mev per emitted neutron.[8,11] The data for the reactions $Pr^{141}(C^{12},4n)Tb^{149g}$ and $Nd^{146}(B^{11},8n)Tb^{149g}$ are shown in Fig. 8. This difference may be due to differences in the energy dissipated by photon emission. If this explanation is correct then total photon energies of $\approx$ 10 to 25 Mev must be emitted with high probability from the Dy compound nuclei. The competition between photon and particle emission has not been adequately predicted theoretically. We will use angular-distribution measurements to deduce the average energy emitted as photons for the various reactions studied.

C. Angular Distributions

From the average recoil range measurements we have concluded that all the reactions studied here proceed by compound-nucleus formation. Furthermore, the range measurements demand that the angular distribution of the emitted neutrons must be essentially symmetric about $\pi/2$ in the moving frame of reference. We will use angular-distribution measurements to deduce information about the properties of the excited compound nuclei.

The angular distribution of the final products depends on the energy and angular distributions of the emitted neutrons (see Sec. II). If the neutrons are emitted as s waves then their emission is isotropic. However, if neutrons are emitted with nonzero ℓ values, then forward-backward peaking is expected. The classical limit to this forward-backward preference is given

by an angular distribution of the form

$$W(\theta) \propto 1/\sin\theta .$$

Experimental studies of heavy-ion reactions have shown that alpha particles and fission fragments are emitted with forward-backward preferences approaching the classical limit.[7,19] Neutrons and protons are emitted with much less forward-backward peaking.[20]

The measured angular distributions may be compared with calculations based on compound-nucleus formation and the statistical model. The most important features of this comparison may be illustrated by reference to the average angle $\langle\theta_L\rangle$ and the root mean square angle $\langle\theta_L^2\rangle^{1/2}$.

Comparisons of measured and calculated values of the average angle are shown in Fig. 9. The calculations are described in some detail in references 12 and 21. Briefly, the evaporation stage is described by the level density D of a Fermi gas:

$$D = \exp\left[2a(E_x - \delta)\right]^{1/2} ,$$

where a is the "level density" parameter and δ is the "characteristic level." No effects of angular momentum are included. For excitation energies greater than the sum of binding and effective-barrier energies, photon emission is taken as negligible. Thus the calculated average energy emitted as photons is always less than about 10 Mev. The calculated results shown in Fig. 9 were obtained by the Monte Carlo method with the two extreme angular distributions: (a) $W(\theta) = 1$ (isotropic), and (b) $W(\theta) \propto 1/\sin\theta$ (limiting anisotropic).

It is clear from Fig. 9 that the calculation gives a reasonably good representation of the decay of Tb compound nuclei to 4.1-hr Tb^{149g}. As stated in the introduction, these reactions probably involve only those compound nuclei of low spin.

The calculation does not agree at all with the measurements for Dy^{149}, Dy^{150}, or Dy^{151} produced from Dy compound nuclei. This disagreement is attributed to effects of the high angular momenta of the compound nuclei. In the calculation no account is taken of angular momentum. Increased probability for photon emission is one possible effect of high angular momentum. The experimental results of Mollenauer indicate that much energy is released as photons from excited nuclei of high angular momentum.[22] The measurements of Morton et al. lend support to this observation.[17] In this work we report more detailed angular-distribution measurements for a number of reactions. We will use these measurements to deduce the average energy dissipated by photon emission as a function of incident energy for these specific reactions.

Let us assume initially that all neutrons are emitted isotropically. From Eqs. (11), (14), (15), and (16) we can calculate the average energy emitted as photons, and the average kinetic energy of the neutrons for each reaction. The results of these calculations are given in Table V.

First we give the bombarding energy; then the available energy in the c.m. system, the average kinetic energy of the neutrons, and average total photon energy. We give both the total energies and the energy per nucleon emitted in the various reactions.

If the neutrons are not emitted isotropically the true energies will differ from those given in Table V. The maximum alteration due to this effect can be evaluated from the Monte Carlo evaporation calculations that compare isotropic emission and extreme forward-backward anisotropy.[12] The Monte Carlo calculations indicate that $\langle \theta_L^2 \rangle^{1/2}$ for isotropic neutron emission is $\approx 15\%$ greater than for $W(\theta) \propto 1/\sin\theta$. Thus if all the neutrons are emitted with this extremely anisotropic angular distribution, then the neutron kinetic energies should be increased by $\approx 32\%$ (see Eq. 18). Also, the total photon energies should be correspondingly decreased (see Eq. 16). Experimental

measurements and theoretical considerations lead one to expect that the approximation of isotropy is more nearly correct than $W(\theta) \propto 1/\sin\theta$.[6,20] In this report we proceed with the discussion based on the approximation of isotropy. For this reason the neutron energies in Table V are probably somewhat too small, and the photon energies are too large. However, these errors are systematic, and thus the dependence on reaction type and bombarding energy is probably correct.

In Fig. 10 we plot the average total photon energy T_γ against the total available energy. There is a drastic difference between the reactions leading to $Dy^{149,150,\text{ and }151}$ and those leading to Tb^{149g}. Increasing the available energy leads to only slightly increased photon energy for Tb^{149g} reactions. But for Dy reactions most of the available energy greater than about 10 or 15 Mev is dissipated by photon emission.

The reactions leading to Tb^{149g} probably involve only systems of low angular momentum, and photon emission does not compete favorably with neutron emission. The reactions leading to $Dy^{149,150,\text{ and }151}$ have very high cross sections (see Fig. 6); thus the observed products must be formed from compound nuclei that have an angular momentum distribution typical of all compound systems. Presumably, this primary angular-momentum distribution gives rise to a large number of compound nuclei of high spin.[18] Angular-momentum barriers prevent neutrons from dissipating much of this angular momentum, so cascades of photons are required to deexcite the compound systems.

Another way of presenting this same information is to plot the average energies per emitted neutron versus the available energy per neutron. These plots are shown in Fig. 11.

The Tb^{149g} reactions give results that are expected from evaporation theory without angular momentum effects. Increasing available energy goes

mainly into neutron kinetic energy. For Dy reactions the average kinetic energy of the neutrons increases only slightly with available energy. For the smaller available energies almost no energy goes to photons. For the higher available energies the photon and neutron energies are comparable.

For Dy reactions these average energies per neutron are only slightly dependent on the number of emitted neutrons. The average neutron energy seems to increase slightly from the reactions (HI,5n)Dy^{151} to (HI,7n)Dy^{149}. This increase reflects the dependence of the so called "nuclear temperature" on excitation energy. The excitation energies for peak cross sections are at $\approx$ 70 and $\approx$ 100 Mev for the (HI,5n) and (HI,7n) reactions, respectively (see Fig. 6). Both excitation functions peak at an available energy of $\approx$ 5.5 Mev/neutron. The corresponding average neutron energies are $\approx$ 2.7 and 3.1 Mev/neutron, respectively.

D. Conclusions

To summarize this study we may list the following conclusions: (a) The reactions involving neutron emission that we have studied proceed by compound-nucleus formation, (b) The decay of Dy^{156} excited to 65 to 125 Mev is almost the same for C^{12} + Nd^{144} and O^{16} + Ce^{140}. (c) Compound nuclei of low spin (as measured by reactions forming Tb^{149g}) have very different decay properties from those of high spin (as measured by reactions forming Dy^{149}, Dy^{150}, and Dy^{151}). (d) The low-spin compound systems dissipate less than $\approx$ 10 Mev in photons; the remaining energy appears as kinetic energy of the emitted neutrons. (e) The higher spin compound systems dissipate, on the average, about one fourth their excitation energy by photon emission. (f) For these systems the average total photon energy per emitted neutron increases almost linearly with the available energy per neutron. This relationship is very similar for reactions in which 5, 6, or 7 neutrons are emitted.

FOOTNOTES AND REFERENCES

* Work done under the auspices of the U. S. Atomic Energy Commission

† On leave from Laboratorie Joliot Curié de Physique Nucléaire Orsay, France.

‡ Present address: Nouvelle Faculté des Sciences de Bordeaux, Talence (Gizonde) France.

1. R. D. Macfarlane, Alpha-Emitting Isomeric State of Tb^{149}, Lawrence Radiation Laboratory Report UCRL-9870, November 1961, Phys. Rev. (in press).
2. R. D. Evans, The Atomic Nucleus (McGraw-Hill Book Company, Inc., New York, 1955).
3. R. Serber, Phys. Rev. 72, 1114 (1947).
4. N. Bohr, Science 86, 161 (1937).
5. J. Blatt and V. F. Weisskopf, Theoretical Nuclear Physics (John Wiley and Sons, Inc., New York, 1952).
6. L. Wolfenstein, Phys. Rev. 82, 690 (1951); see also T. Ericson and V. Struntinski Nuclear Phys. 8, 284 (1958).
7. W. J. Knox, A. R. Quinton, and C. E. Anderson, Phys. Rev. 126, 2120 (1960).
8. L. Winsberg and J. M. Alexander, Phys. Rev. 121, 518 and 529 (1959).
9. P. F. Donovan, B. G. Harvey, and W. H. Wade, Phys. Rev. 119, 218 and 225 (1960).
10. J. M. Alexander and D. H. Sisson, Lawrence Radiation Laboratory Report UCRL-10098 (unpublished).
11. J. M. Alexander, Lawrence Radiation Laboratory, University of California, Berkeley (unpublished data).
12. J. M. Alexander, L. Altman, and S. Howry, Lawrence Radiation Laboratory, University of California, Berkeley (unpublished).
13. L. Winsberg, Bull. Am. Phys. Soc. 3, 406 (1958).

FOOTNOTES AND REFERENCES (cont)

14. R. D. Macfarlane, Lawrence Radiation Laboratory, University of California, Berkeley (unpublished data).

15. L. C. Northcliffe, Phys. Rev. 120, 1744 (1960).

16. John Walton, Lawrence Radiation Laboratory, University of California, Berkeley (private communication).

17. J. R. Morton, Investigation of Nuclear Reactions by Recoil Studies of Radioactive Products (Ph.D. Thesis), Lawrence Radiation Laboratory Report UCRL-9595. April 1961 (unpublished).

18. T. D. Thomas, Phys. Rev. 116, 703 (1959).

19. Victor E. Viola, Angular Distribution from Heavy-Ion-Induced Fission (Ph.D. Thesis), Lawrence Radiation Laboratory Report UCRL-9619 April 1961 (unpublished).

20. H. W. Broek, Phys. Rev. 124, 233 (1961).

21. I. Dostrovsky, Z. Fraenkel, and G. Friedlander, Phys. Rev. 116, 683 (1959).

22. J. F. Mollenauer, Effects of Angular Momentum on Gamma-Ray Production in Compound Nucleus Reactions, Lawrence Radiation Laboratory Report UCRL-9724, June 1960 (unpublished).

Table I. Range measurements in Al.

Reaction	Laboratory bombarding energy, E_b (Mev)	Observed product	Average range, R_o (mg/cm^2)	Measured struggling parameter, ρ	Nuclear reaction straggling parameter, ρ_n [a]
$Ce^{140} + O^{16}$	146.0	Tb^{149}	0.996	0.183	0.09±0.035
		Dy^{150}	0.991	0.190	0.102±0.03
	140.0	Tb^{149}	0.953	0.186	0.083±0.04
		Dy^{150}	0.958	0.197	0.105±0.03
	128.1	Tb^{149}	0.910	0.196	0.089±0.033
		Dy^{150}	0.912	0.202	0.10±0.03
	112.4	Tb^{149}	0.803	0.193	≈ 0
	100.4	Dy^{151}	0.758	0.200	≈ 0
	100.0	Dy^{151}	0.730	0.196	≈ 0
	88.2	Dy^{151}	0.677	0.199	≈ 0
$Nd^{144} + C^{12}$	120.5	Tb^{149}	0.661	0.245	0.082±0.03
		Dy^{150}	0.656	0.248	0.085±0.03
	95.0	Tb^{149}	0.549	0.224	≈ 0
		Dy^{150}	0.551	0.223	≈ 0
		Dy^{151}	0.554	0.237	≈ 0

[a] The value of ρ_n is given only if it is significantly different from zero.

Table II. Cross-section Data.

Laboratory bombarding energy, E_b (Mev)	Cross section, σ (mb)	Fraction of reaction cross section, σ/σ_R [a]
$Nd^{146}(B^{11},8n)Tb^{149g}$		
112.8	6.89	0.0030
108.5	9.19	0.0041
105.6	11.5	0.0052
102.7	13.4	0.0062
97.9	12.7	0.0061
94.5	10.6	0.0052
91.5	7.84	0.0040
88.0	4.66	0.0025
84.5	2.17	0.0012
81.0	1.11	0.0006
$Nd^{144}(C^{12},5n)Dy^{151}$		
76.3	189	0.153
81.7	472	0.334
87.0	591	0.376
92.0	537	0.314
96.8	437	0.238
101.5	292	0.155
106.1	142	0.073
110.5	68	0.034
114.5	34	0.016
$Nd^{144}(C^{12},6n)Dy^{150}$		
76.3	11.8	0.010
81.7	43.3	0.031
87.0	164	0.104
92.0	381	0.223

Table II. Cross-section Data (cont)

Laboratory bombarding energy, E_b (Mev)	Cross section, σ (mb)	Fraction of reaction cross section, σ/σ_R [a]
$Nd^{144}(C^{12},6n)Dy^{150}$ (cont)		
96.8	656	0.357
101.5	783	0.415
106.1	830	0.427
110.5	705	0.352
114.5	554	0.267
122.8	274	0.126
95.0	537	0.303
122.8	290	0.133
$Nd^{144}(C^{12},7n)Dy^{149}$ (by Tb^{149g})		
87.0	5.2	0.003
92.0	10.9	0.006
96.8	36.7	0.020
101.5	82.0	0.044
106.1	149	0.076
110.5	214	0.107
114.5	262	0.126
118.8	282	0.133
122.8	280	0.129
95.0	27.2	0.015
122.8	300	0.138
$Ce^{140}(O^{16},5n)Dy^{151}$		
82.7	28.7	0.035
93.8	331	0.288
104.2	487	0.340
113.8	349	0.207
131.4	48	0.024

Table II. Cross-section Data (cont)

Laboratory bombarding energy, E_b (Mev)	Cross section σ (mb)	Fraction of reaction cross section, σ/σ_R [a]
$Ce^{140}(O^{16},6n)Dy^{150}$		
93.8	17	0.015
104.2	255	0.178
113.8	497	0.296
131.4	441	0.224
151.7	79	0.036
163.0	17	0.007
$Ce^{140}(O^{16},7n)Dy^{149}$ (by Tb^{149g})		
113.8	51.5	0.031
131.4	240	0.122
151.7	162	0.073
163.0	71	0.031

[a] Total reaction cross sections were obtained by interpolation of the calculated results in reference 18.

Table III. Angles defined by each cutting edge (deg).[a]

Ring number	Cutter 1	Cutter 2
	0	0
1	1.16	1.04
2	2.10	2.04
3	3.12	3.07
4	4.15	4.12
5	5.16	5.15
6	6.16	6.18
7	7.15	7.17
8	8.17	8.21
9	9.19	9.19
10	10.19	10.19
11	11.18	11.16
12	12.13	12.15
13	13.14	13.17
14	14.15	14.10
15	15.08	15.08
16	16.02	16.06

[a] For each ring the inner and outer angles are given. The outer angle for any ring is the inner angle for the next.

Table IV. Angular distribution results. (cont)

Laboratory bombarding energy, E_b (Mev)	Target thickness, W($\mu g/cm^2$)	Cutter	Fractional cross section per unit angle, $\Delta\sigma/\sigma\Delta\theta$ (deg^{-1}) — Ring number → 1	2	3	4	5	6	7	8	9	10	11	12	13	14	15	16	17	18	$\langle\theta_L\rangle$	$\langle\theta_L^2\rangle^{1/2}$
			$Nd^{144}(C^{12},7n)Dy^{149}$																				
94.0	30.9	1	(0.054)	0.085	0.119	0.152	0.146	0.120	0.106	0.077	0.046	0.028	0.018	0.014	0.011	(0.006)	(0.004)						5.03	5.76
94.0	0																						4.66	5.35
99.7	30.9	2	← 0.067 →		0.121	0.139	0.143	0.129	0.103	0.075	0.051	0.035	← 0.016 →		0.008	0.006	(0.003)						5.05	5.80
99.7	0																						4.68	5.39
111.6	30.9	1	0.034	0.082	0.118	0.139	0.138	0.126	0.103	0.088	0.057	0.039	← 0.020 →		0.012	(0.008)	(0.005)	(0.004)					5.40	6.15
111.6	0																						5.03	5.74
122.8	10.8	1	← 0.058 →		← 0.125 →		0.141	0.126	0.110	0.084	0.063	0.040	← 0.022 →		0.008	0.004	0.002						5.21	6.01
122.8	30.9	2	← 0.051 →		← 0.121 →		0.135	0.126	0.111	0.086	0.065	0.046	← 0.022 →		0.012	0.007	0.004						5.48	6.22
122.8	76.8	1	← 0.046 →		← 0.111 →		0.120	0.122	0.105	0.091	0.069	0.053	← 0.032 →		0.018	0.012	0.009	0.006	(0.004)	(0.003)			6.01	6.88
122.8	0		← 0.057 →		← 0.127 →		0.145	0.128	0.110	0.083	0.062	0.039	← 0.018 →		0.007	0.003	0.0015						5.09	5.84
			$Ce^{140}(O^{16},5n)Dy^{151}$																				
89.7	36.4	2	0.062	0.142	0.187	0.188	0.167	0.100	0.063	0.030	0.014	0.010	0.006	0.006									3.85	4.40
89.7	0																						3.63	4.16
101.0	36.4	1	0.053	0.142	0.186	0.189	0.145	0.113	0.075	0.048	0.019	0.011	0.004	0.002									4.00	4.53
101.0	0																						3.78	4.27
111.0	21.0	2	0.045	0.129	0.177	0.184	0.159	0.120	0.079	0.043	0.020	0.011	0.005	0.002	0.001								4.08	4.70
111.0	0																						3.95	4.55
			$Ce^{140}(O^{16},6n)Dy^{150}$																				
101.0	36.4	1	0.063	0.134	0.166	0.183	0.167	0.120	0.079	0.024	0.032	0.008	0.008	0.004									4.03	4.59
101.0	0																						3.81	4.33
111.0	21.0	2	0.045	0.129	0.177	0.184	0.159	0.120	0.079	0.043	0.020	0.011	0.005	0.002	0.001								4.08	4.70
111.0	0																						3.95	4.55
121.1	36.4	2	0.047	0.114	0.151	0.177	0.166	0.131	0.080	0.054	0.040	0.021	0.013	0.006									4.44	5.06
121.1	0																						4.22	4.80
130.4	36.4	2	0.038	0.110	0.158	0.177	0.153	0.124	0.089	0.059	0.036	0.022	0.007	0.003									4.42	4.97
130.4	0																						4.20	4.71
139.2	21.0	2	0.040	0.108	0.164	0.171	0.160	0.120	0.094	0.055	0.033	0.019	0.008	0.003									4.37	4.92
139.2	0																						4.24	4.77

Table IV. Angular distribution results.

Laboratory bombarding energy, E_b (Mev)	Target thickness, W($\mu g/cm^2$)	Cutter	Fractional cross section per unit angle, $\Delta\sigma/\sigma\Delta\theta$ (deg^{-1}) — Ring number 1	2	3	4	5	6	7	8	9	10	11	12	13	14	15	16	17	18	$\langle\theta_L\rangle$	$\langle\theta_L^2\rangle^{1/2}$
											$Pr^{141}(C^{12},4n)Tb^{149g}$												
>57.7[a]	27.2	2[b]	0.046	0.107	0.155	0.169	0.149	0.121	0.090	0.055	0.039	0.020	0.012	0.007	(0.004)[c]	(0.002)					4.51	5.15
>57.7	0																				3.95	4.49
67.8	27.2	2[b]	0.033	0.089	0.132	0.149	0.150	0.133	0.100	0.074	0.045	0.030	0.018	0.012	0.008	0.005					4.97	5.64
67.8	0																				4.41	4.98
											$Nd^{146}(B^{11},8n)Tb^{149g}$											
90.2	27.4	2[b]	(0.059)	0.078	0.095	0.114	0.126	0.122	0.101	0.088	0.062	0.056	0.034	0.019	0.012	0.008	(0.005)	(0.003)			5.54	6.37
90.2	0																				5.11	5.83
103.7	27.4	2	(0.025)	0.047	0.073	0.099	0.104	0.112	0.109	0.112	0.074	0.075	0.051	0.037	0.028	0.013	0.010	(0.007)	(0.005)	(0.003)	6.69	7.53
103.7	89.0	1	(0.026)	0.046	0.069	0.090	0.099	0.108	0.101	0.096	0.081	0.071	0.057	0.043	0.037	0.023	0.017	(0.011)	(0.008)	(0.006)	7.13	8.07
103.7	0		0.025	0.048	0.074	0.100	0.107	0.113	0.111	0.110	0.078	0.075	0.048	0.034	0.024	0.008					6.50	7.29
112.8	27.4	1	(0.027)	0.043	0.067	0.083	0.101	0.113	0.108	0.094	0.085	0.075	0.053	0.044	0.036	0.025	0.013	(0.011)	(0.007)	(0.005)	7.13	8.04
112.8	0																				6.94	7.80
											$Nd^{144}(C^{12},5n)Dy^{151}$											
77.5	77.0	2	0.036	0.086	0.123	0.140	0.137	0.115	0.096	0.074	0.052	0.038	0.025	0.018	0.015	0.011	(0.007)	(0.005)	(0.004)		5.39	6.26
77.5	77.0	1[b]	0.039	0.080	0.116	0.139	0.127	0.119	0.101	0.076	0.054	0.041	0.027	0.021	0.015	0.014	(0.008)	(0.006)	(0.004)	(0.003)	5.63	6.56
77.5	0																				4.48	5.36
83.4	30.9	2	0.040	0.100	0.135	0.149	0.140	0.117	0.105	0.075	0.047	0.029	0.014	0.013	0.010	(0.005)	(0.003)				4.94	5.66
83.4	0																				4.57	5.25
94.0	30.9	1	0.050	0.089	0.114	0.129	0.133	0.137	0.101	0.080	0.059	0.037	0.024	0.013	0.010	(0.006)	(0.004)	(0.003)			5.25	5.88
94.0	0																				4.88	5.47
											$Nd^{144}(C^{12},6n)Dy^{150}$											
94.0	30.9	1	0.048	0.088	0.114	0.146	0.149	0.117	0.099	0.072	0.048	0.037	0.027	(0.017)	(0.012)	(0.008)	(0.006)	(0.004)			5.24	6.04
94.0	0																				4.87	5.64
99.7	30.9	2	← 0.054 →		← 0.129 →		0.147	0.131	0.107	0.082	0.061	0.038	← 0.014 →		0.012	0.006	(0.003)				5.22	5.93
99.7	0																				4.85	5.52
111.6	30.9	1	←0.049 →		← 0.120 →		0.133	0.133	0.109	0.086	0.066	0.045	← 0.024 →		0.012	0.008	0.005	(0.003)			5.56	6.33
111.6	0																				5.19	5.92
122.8	76.8	1	←0.044 →		← 0.096 →		0.115	0.126	0.106	0.092	0.078	0.058	← 0.037 →		0.029	0.016	0.012	0.005			6.24	7.09
122.8	0																				5.32	6.06

Table IV. Angular distribution results. (cont)

Laboratory bombarding energy, E_b (Mev)	Target thickness $W(\mu g/cm^2)$	Cutter	Fractional cross section per unit angle, $\Delta\sigma/\sigma\Delta\theta$ (deg^{-1}) — Ring number →																	$\langle\theta_L\rangle$	$\langle\theta_L^2\rangle^{1/2}$
			1	2	3	4	5	6	7	8	9	10	11	12	13	14	15	16	17	18	
$Ce^{140}(O^{16},7n)Dy^{149}$																					
111.0	21.0	2	0.043	0.120	0.161	0.172	0.158	0.120	0.086	0.055	0.030	0.016	0.007	0.005	0.002	0.0006					4.33	4.91
111.0	72.8	1	0.043	0.107	0.150	0.163	0.153	0.126	0.094	0.064	0.037	0.022	0.013	0.007	0.005	0.004					4.64	5.28
111.0	0		0.043	0.125	0.165	0.175	0.160	0.118	0.083	0.051	0.027	0.014	0.006	0.004	0.0004						4.20	4.76
121.1	36.4	1	0.045	0.122	0.154	0.170	0.158	0.128	0.092	0.058	0.034	0.013	0.010	0.006							4.39	4.96
121.1	0																				4.17	4.70
130.4	21.0	2	0.043	0.113	0.157	0.171	0.156	0.127	0.088	0.061	0.033	0.018	0.008	0.004							4.38	4.95
130.4	36.4	1	0.047	0.114	0.157	0.169	0.156	0.125	0.093	0.058	0.035	0.020	0.008	0.007							4.43	5.01
130.4	0		0.038	0.111	0.157	0.172	0.156	0.127	0.083	0.060	0.030	0.015	0.007	0.001							4.21	4.75
139.2	36.4	1	0.046	0.110	0.153	0.166	0.153	0.135	0.091	0.059	0.037	0.019	0.009	0.007	0.003						4.50	5.09
139.2	0																				4.26	4.81
163.0	36.4	1	0.039	0.091	0.130	0.149	0.146	0.135	0.110	0.077	0.053	0.030	0.017	0.009	0.003						4.93	5.55
163.0	0																				4.71	5.29

[a] A few of the energy-degrading foils burned out during this experiment.

[b] The second collimator was 1/8-in.

[c] Values in parentheses were obtained by graphical extrapolation.

Table V. Average energies (in Mev) from $\langle \theta_L^2 \rangle^{1/2}$, assuming isotropic emission of neutrons.

Laboratory bombarding energy, E_b	Available energy, $E_{c.m.} + Q$		Average kinetic energy of neutrons		Average energy dissipated by photons	
	total	per neutron	total	per neutron	total	per neutron
		$Pr^{141}(C^{12},4n)Tb^{149g}$				
> 58 [a]	8.3	2.075	6.2	1.55	2.1	0.55
67.8	17.3	4.33	9.0	2.25	8.3	2.08
		$Nd^{146}(B^{11},8n)Tb^{149g}$				
90.2	20.0	2.50	14.6	1.82	5.4	0.68
103.7	32.5	4.06	26.3	3.29	6.2	0.78
112.8	41.0	5.13	32.8	4.10	8.2	1.02
		$Nd^{144}(C^{12},5n)Dy^{151}$				
77.5	17.4	3.48	11.1	2.22	6.3	1.26
83.4	22.9	4.58	12.2	2.44	10.7	2.14
94.0	32.7	6.54	14.9	2.98	17.8	3.56
		$Nd^{144}(C^{12},6n)Dy^{150}$				
94.0	24.9	4.15	15.8	2.63	9.1	1.52
99.7	30.1	5.02	16.0	2.67	14.1	2.35
111.6	41.1	6.85	20.6	3.43	20.5	3.42
122.8	51.5	8.58	23.8	3.97	27.7	4.62
		$Nd^{144}(c^{12},7n)Dy^{149}$				
94.0	15.6	2.23	14.1	2.01	1.5	0.21
99.7	20.8	2.97	15.2	2.17	5.6	0.80
111.6	31.8	4.54	19.3	2.76	12.5	1.79
122.8	42.2	6.03	21.9	3.13	20.3	2.90

Table V. Average energies (in Mev) from $\langle \theta_L^2 \rangle^{1/2}$, assuming isotropic emission of neutrons. (cont)

Laboratory bombarding energy, E_b	Available energy, $E_{c.m.} + Q$		Average kinetic energy of neutrons		Average energy dissipated by photons	
	total	per neutron	total	per neutron	total	per neutron
		$Ce^{140}(O^{16},5n)Dy^{151}$				
89.7	17.4	3.48	11.0	2.20	6.4	1.28
101.0	27.5	5.50	13.0	2.60	14.5	2.90
111.0	36.5	7.30	16.1	3.22	20.4	4.08
		$Ce^{140}(O^{16},6n)Dy^{150}$				
101.0	19.7	3.28	13.3	2.22	6.4	1.07
111.0	28.7	4.78	16.1	2.68	12.6	2.10
121.1	37.8	6.30	19.6	3.27	18.2	3.03
130.4	46.1	7.68	20.3	3.38	25.8	4.30
139.2	54.0	9.00	22.3	3.72	31.7	5.28
		$Ce^{140}(O^{16},7n)Dy^{149}$				
111.0	19.4	2.77	17.8	2.54	1.6	0.23
121.1	28.5	4.07	19.0	2.71	9.5	1.36
130.4	36.8	5.26	20.9	2.99	15.9	2.27
139.2	44.7	6.39	23.0	3.29	21.7	3.10
163.0	66.1	9.44	32.3	4.61	33.8	4.83

[a] A few of the energy-degrading foils burned out during this experiment.

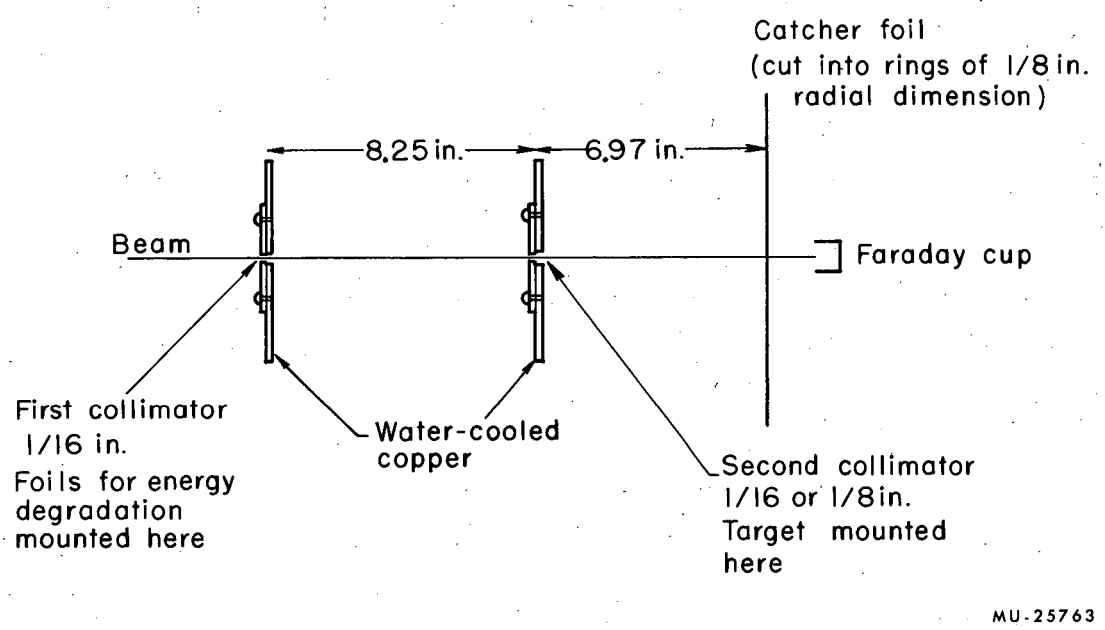

Fig. 1. Schematic diagram of the apparatus used for angular-distribution measurements.

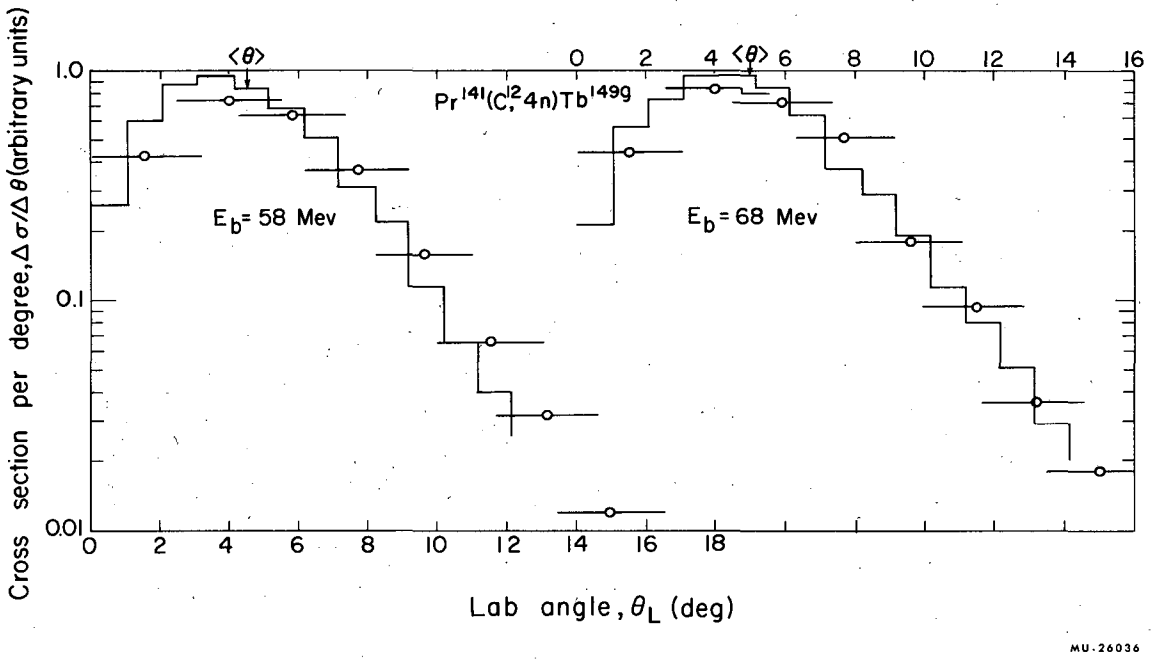

Fig. 2. Comparison of angular-distribution measurements for the reaction $Pr^{141}(C^{12},4n)Tb^{149g}$. The histograms are from this work (see Table IV). The points are from reference 17; the bars indicate lower limits to the angular resolution. (Target thicknesses were about 27μg/cm^2 in all experiments.)

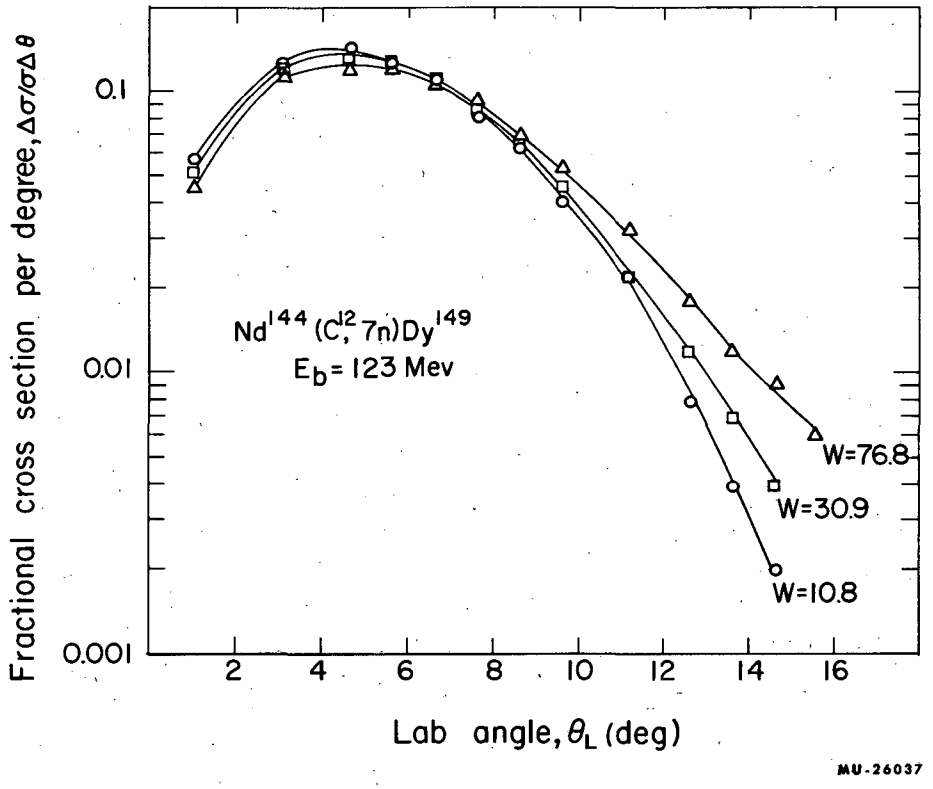

Fig. 3. The effect of target thickness on observed angular distribution. The target thickness W is denoted for each curve in $\mu g/cm^2$. These data are for the reaction Nd^{144} + 123-Mev $C^{12} \rightarrow Dy^{149}$ + 7n.

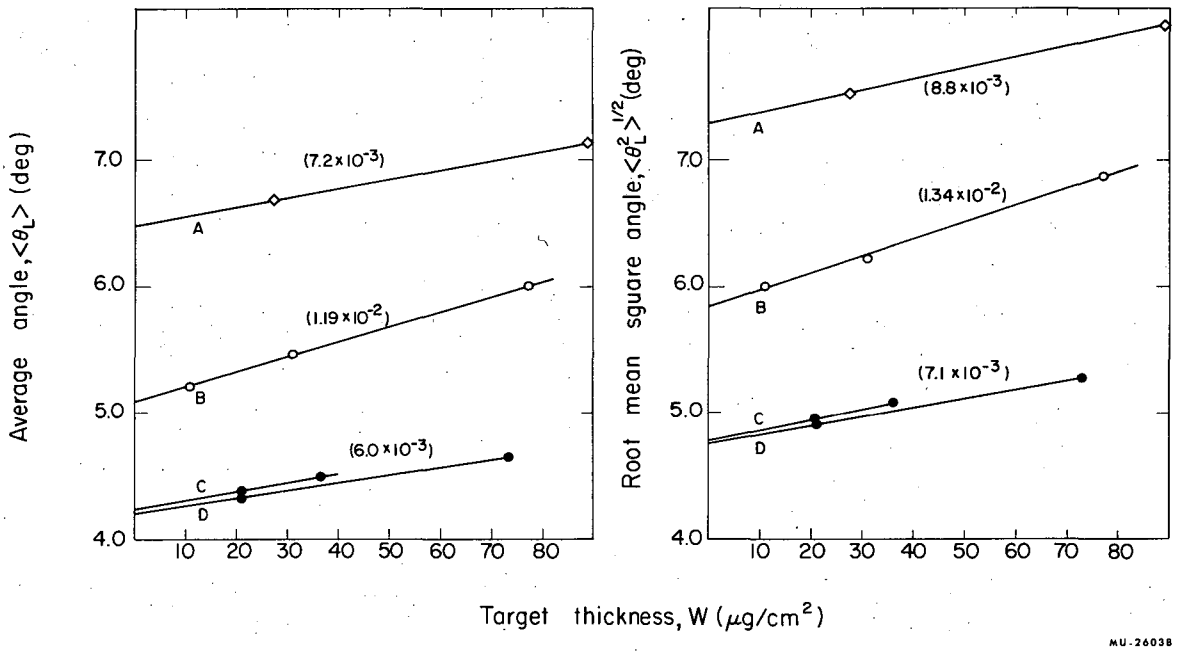

Fig. 4. The dependence of (a) the average angle $\langle\theta_L\rangle$ and (b) the root mean square angle $\langle\theta_L^2\rangle^{1/2}$ on target thickness W. Curves A are for the reaction Nd^{146} + 104-Mev $B^{11} \rightarrow Tb^{149g}$ + 8n;
B for Nd^{144} + 123-Mev $C^{12} \rightarrow Dy^{149}$ + 7n;
C for Ce^{140} + 139-Mev $O^{16} \rightarrow Dy^{149}$ + 7n; and
D for Ce^{140} + 111-Mev $O^{16} \rightarrow Dy^{149}$ + 7n.
The numbers in parentheses denote the slopes of the curves in deg/(μg/cm²).

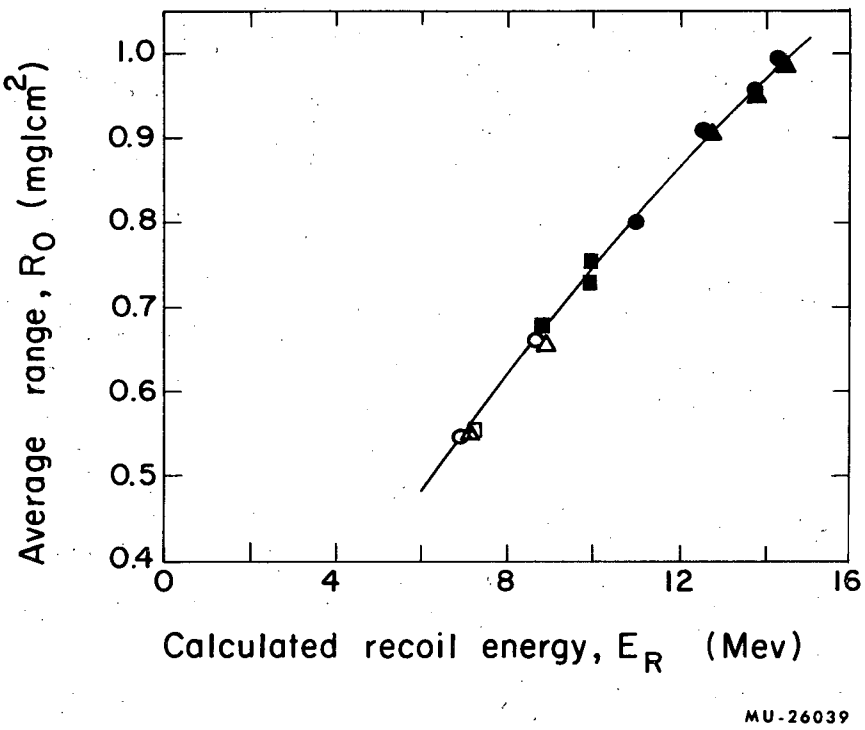

Fig. 5. Average range R_O in Al vs the calculated recoil energy E_R. Symbols are as follows: Dy^{151} ⊡; Dy^{150} △; Dy^{149} ⊙. Open symbols are for the reactions C^{12} + Nd^{144}; closed, for O^{16} + Ce^{140}. The smooth curve is from reference 10.

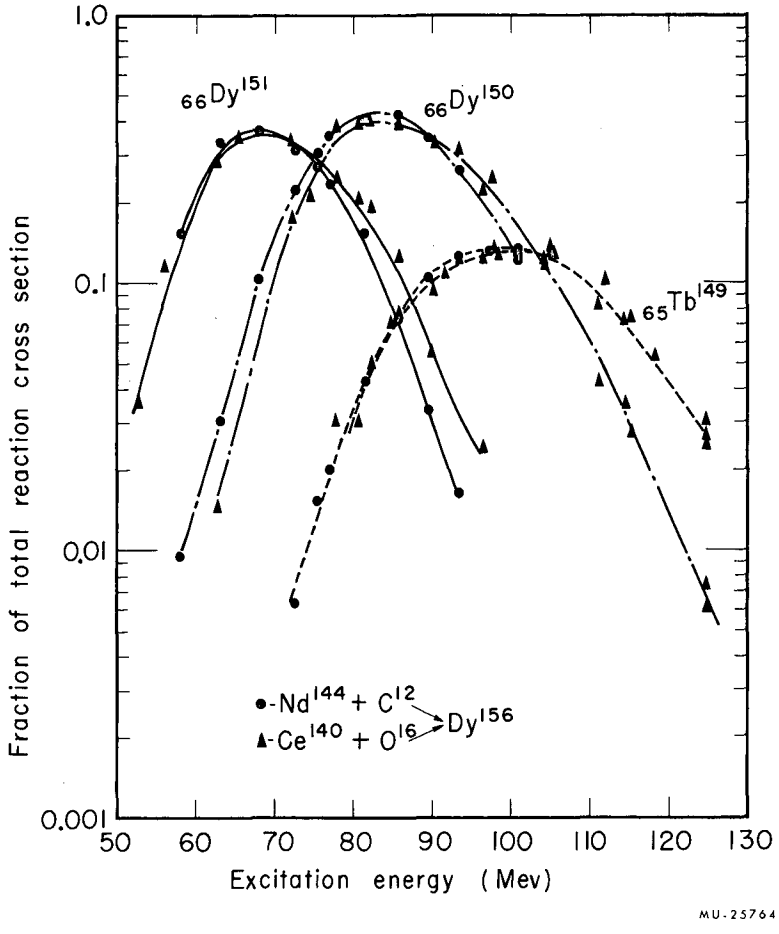

Fig. 6. Fraction of the calculated reaction cross section vs excitation energy. Total reaction cross sections are from reference 18.

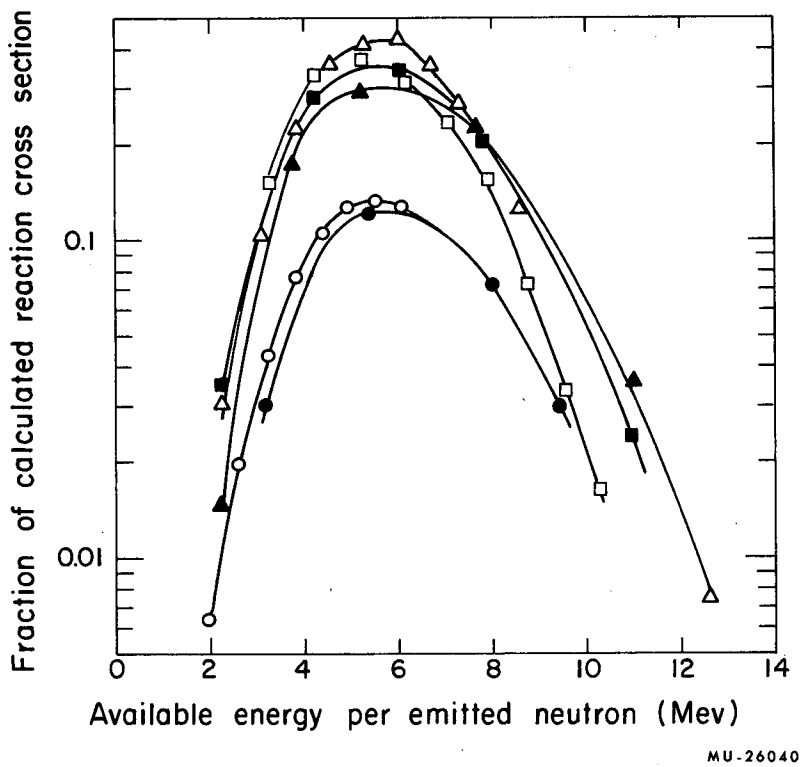

Fig. 7. Fraction of the calculated reaction cross section vs available energy per emitted neutron. The symbols are as in Fig. 5. Total reaction cross sections are from reference 18.

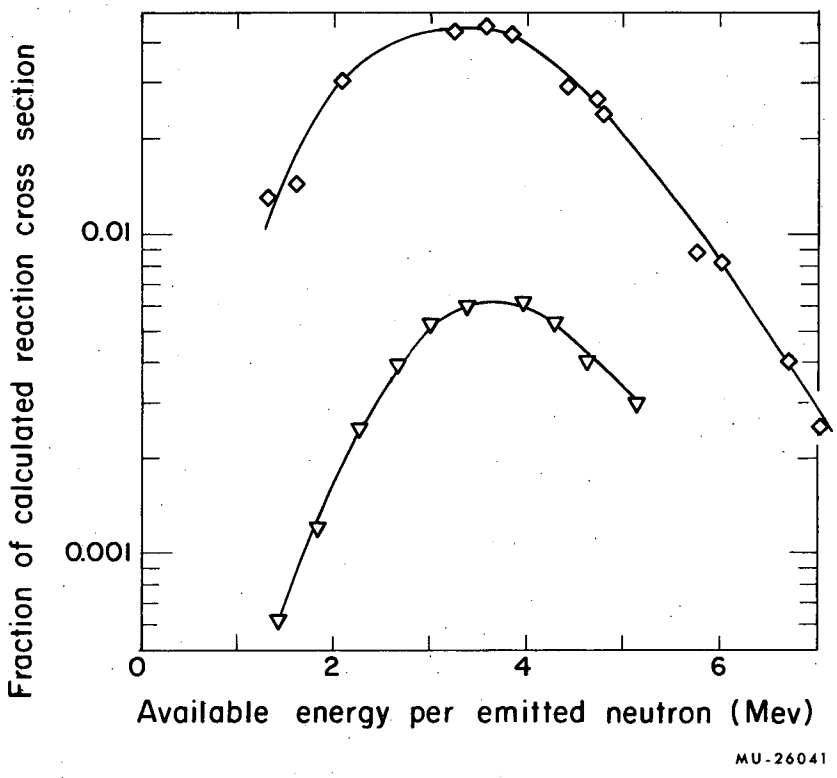

Fig. 8. Fraction of the calculated reaction cross section vs available energy per emitted neutron. The symbols are as follows: $Pr^{141}(C^{12},4n)Tb^{149g}$ ◇; $Nd^{146}(B^{11},8n)Tb^{149g}$ ▽. Total reaction cross sections are from reference 18.

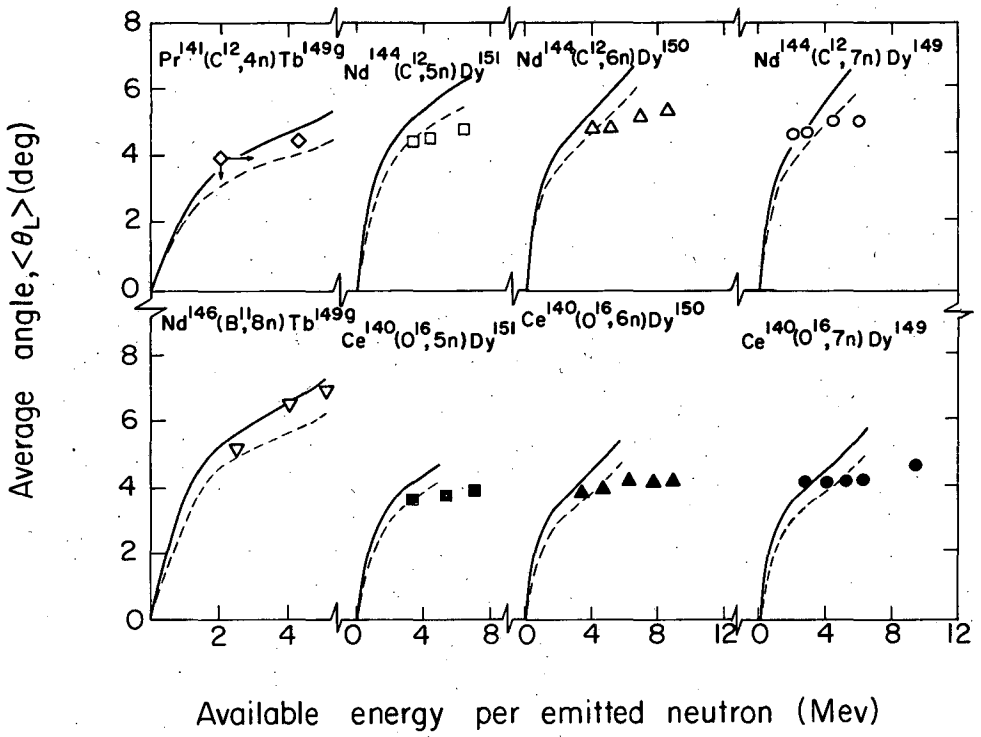

Fig. 9. Dependence of average angle $\langle\theta_L\rangle$ on bombarding energy. The solid curves were calculated for isotropic neutron emission; the dashed curves for neutron angular distribution of $1/\sin\theta$. The points are experimental.

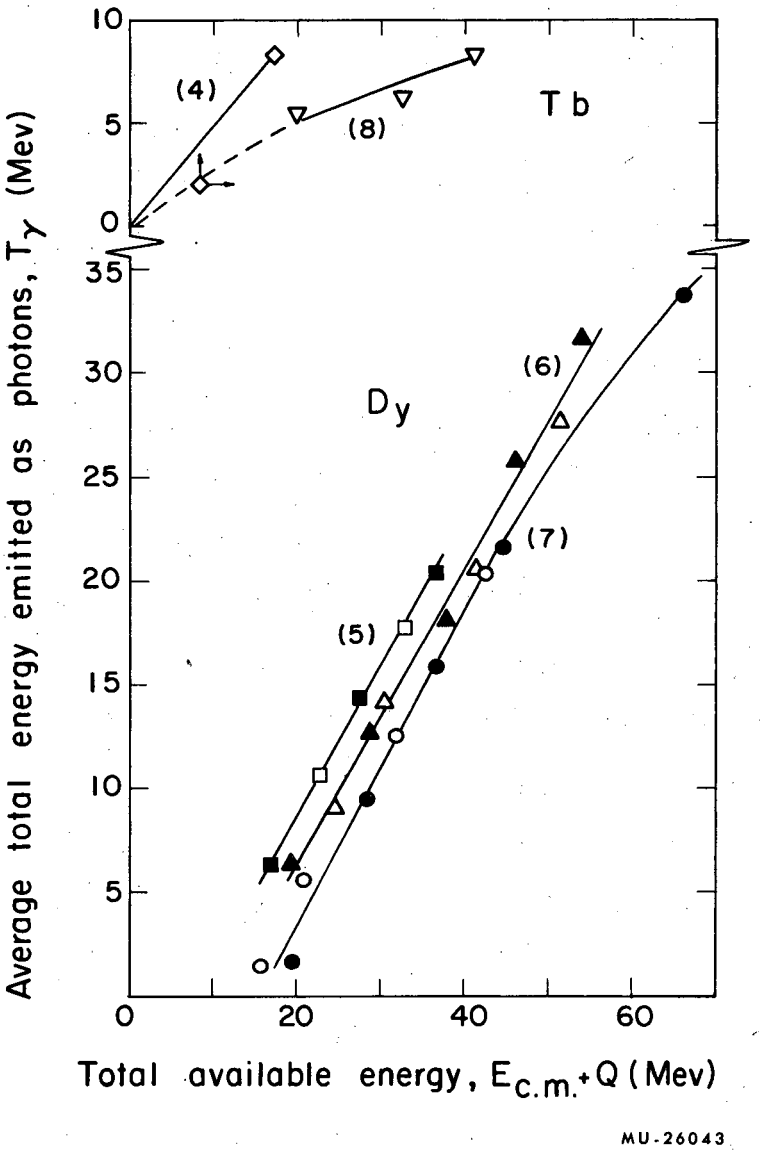

Fig. 10. Total photon energy vs total available energy. The upper curves are for Tb^{149g}; the lower curves for Dy with the same symbols as in Fig. 9. The number of emitted neutrons for each curve is shown in parentheses.

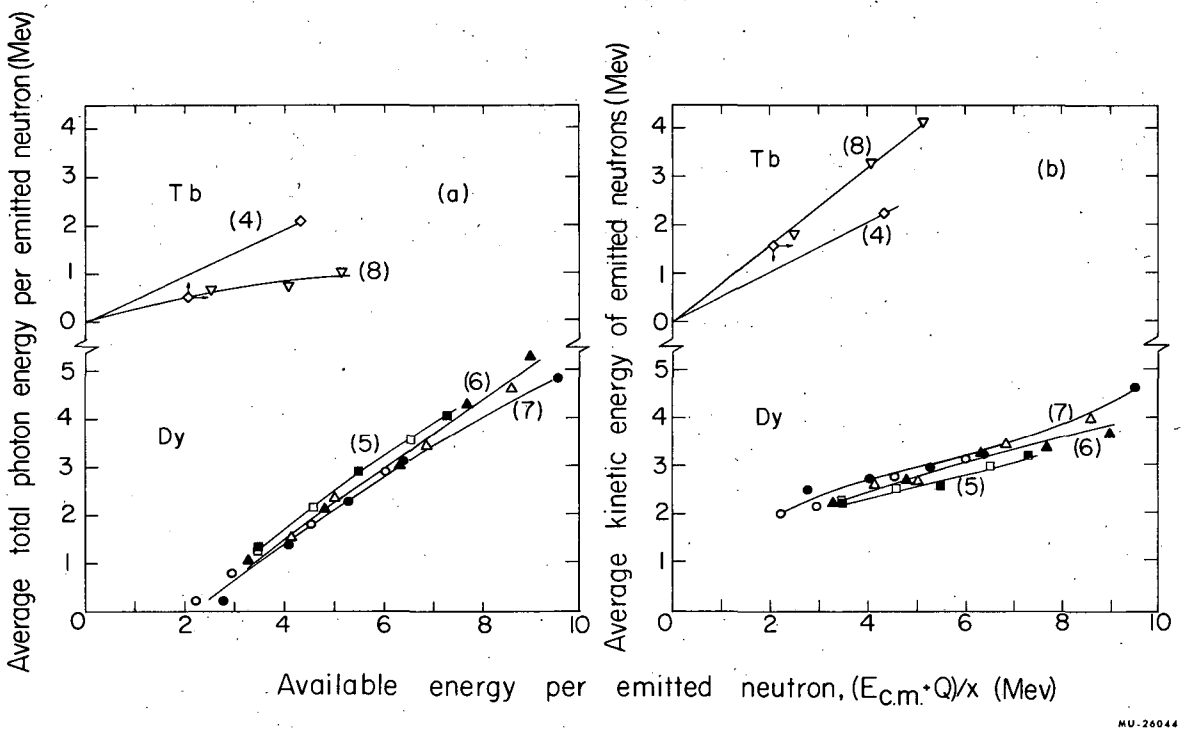

Fig. 11. Average total energy of photons (a) and average neutron energy (b) vs available energy per emitted neutron $(E_{c.m.} + Q)/x$ for reactions in which x neutrons are emitted. Symbols are the same as in Fig. 9.